



Published as: *Nano Lett.* 2013 September 11; 13(9): 4060–4067.

Effect of Particle Diameter and Surface Composition on the Spontaneous Fusion of Monolayer-Protected Gold Nanoparticles with Lipid Bilayers

Reid C. Van Lehn[†], Prabhani U. Atukorale[‡], Randy P. Carney[§], Yu-Sang Yang[†], Francesco Stellacci[§], Darrell J. Irvine^{†,‡,||,⊥}, and Alfredo Alexander-Katz^{*,†}

[†]Department of Materials Science and Engineering, Massachusetts Institute of Technology,

Cambridge, Massachusetts 02139, United States [‡]Department of Biological Engineering,

Massachusetts Institute of Technology, Cambridge, Massachusetts 02139, United States

[§]Institute of Materials, École Polytechnique Federale de Lausanne, 1015 Lausanne, Switzerland

^{||}Koch Institute for Integrative Cancer Research, Massachusetts Institute of Technology,

Cambridge, Massachusetts, 02139, United States [⊥]Howard Hughes Medical Institute, Chevy

Chase, Maryland 20815, United States

Abstract

Anionic, monolayer-protected gold nanoparticles (AuNPs) have been shown to nondisruptively penetrate cellular membranes. Here, we show that a critical first step in the penetration process is potentially the fusion of such AuNPs with lipid bilayers. Free energy calculations, experiments on unilamellar and multilamellar vesicles, and cell studies all support this hypothesis. Furthermore, we show that fusion is only favorable for AuNPs with core diameters below a critical size that depends on the monolayer composition.

Keywords

lipid bilayer; gold nanoparticle; surface monolayer; membrane insertion; cell penetration; snorkeling

Biological cellular membranes are complex, dynamic structures composed of a wide variety of transmembrane proteins, cholesterol, and other biological molecules immersed in a multicomponent lipid bilayer matrix. The plasma membrane acts as a protective barrier for the cell, selectively controlling entry into the cytosol via endocytotic mechanisms triggered by specific ligand–receptor interactions. The membrane's barrier properties are conferred to a large extent by the hydrophobic bilayer interior that prevents the passive permeation of

* Corresponding Author aalexand@mit.edu..

ASSOCIATED CONTENT:

Additional details on nanoparticle synthesis, multilamellar vesicle preparation, bilayer electrical measurements, and simulation methods; TEM measurements of particle size distribution and particle interactions with multilamellar vesicles; additional simulation snapshots and flow cytometry data. This material is available free of charge via the Internet at <http://pubs.acs.org>.

The authors declare no competing financial interest.

charged and polar molecules. However, some short cationic peptides can spontaneously pass through plasma/ endosomal membranes despite bearing surface charges. These peptides can be roughly divided into two classes: antimicrobial peptides and cell-penetrating peptides. Antimicrobial peptides collectively insert into cell membranes to form pores, leading to cytosolic leakage and cell death.¹ Cell-penetrating peptides, also known as Trojan peptides, are able to penetrate into cells. Their mechanism of penetration may vary depending on the specific peptide and is still under debate; in some cases it may involve transient bilayer disruption.^{2,3} Similar to these biological molecules, membrane disruption has also been observed during the spontaneous penetration of functionalized cationic gold nanoparticles (AuNPs).^{4,5} However, the cytotoxicity of cationic AuNPs may limit their utility.

In contrast to cationic peptides and AuNPs that perturb the membrane, it is well-known that there are membrane proteins that nondisruptively reside within lipid bilayers.⁶ These transmembrane proteins are characterized by amphiphilic surfaces that are more stable in the bilayer environment than in aqueous solution. Very recently, some of us showed that AuNPs protected by an amphiphilic monolayer can non-disruptively penetrate the plasma membrane of cells. Surprisingly, penetration is observed even when endocytosis is arrested, implying that the particles enter cells via an energy-independent mechanism with no evidence of membrane poration or cell death.^{7,8} The AuNPs were protected by a binary mixture of hydrophobic and anionic, endfunctionalized alkanethiol ligands that spontaneously separate into stripelike domains.⁹⁻¹¹ Nanoscale morphology plays a key role in controlling cellular penetration, as forcing the ligand shell into a mixed conformation by including branched hydrophobic ligands decreases nonspecific uptake significantly.^{7,12} This spontaneous, nondisruptive translocation is reminiscent of transmembrane proteins and likely depends on a fundamentally different pathway than the penetration of cationic AuNPs. While some recent computational studies have examined the interactions of similar particles with lipid bilayers,¹³⁻¹⁶ to the best of our knowledge no mechanism explaining the non-disruptive penetration of anionic, striped AuNPs through membranes has been identified. We propose that penetration into cells consists of multiple steps: first, the AuNPs must fuse with the membrane in a nondisruptive transmembrane configuration, then from this configuration the AuNPs may translocate into the cell interior. In this work, we focus on understanding the critical first step of membrane fusion and its dependence on particle size, monolayer composition, and ligand morphology. We note that the AuNPs we work with are also highly soluble in aqueous environments, so the observation of fusion indicates that they are able to exhibit wettability toward both water and lipid chains. This property is conferred, as will be shown below, by the flexibility of the ligands and the free volume accessible to them. Such versatility had not been observed before for highly charged nanoparticle systems. As similar monolayer-protected AuNPs are widely utilized in biological applications, understanding this unique fusion process may enable the design of drug delivery devices, biosensors, and biological devices¹⁷⁻¹⁹ and provide insights into the mechanisms of bilayer translocation for charged biological and synthetic materials in general.

To gain a physical understanding of AuNP-membrane interactions, our simplified system consists of well-defined synthetic lipid bilayers and monolayer-protected AuNPs. We use experiments and theory to investigate the hypothesis that membrane penetration involves an

intermediate state in which the anionic AuNP inserts into the lipid bilayer. We propose that insertion is driven by the hydrophobic effect as fusing the AuNP with the bilayer shields hydrophobic ligands within the hydrophobic bilayer core.²⁰ In principle, stable fusion with the bilayer is challenged by the highly charged surfaces of the particles. The striped domains have an average width of 0.6 nm,^{7,10} significantly smaller than the typical thickness of the bilayer core, implying that insertion would expose anionic groups to the bilayer interior in an energetically unfavorable state.^{21,22} However, the monolayers of small AuNPs have large amounts of free volume that grant conformational flexibility to the ligands.²³ This flexibility allows the ligands to deform and “snorkel” charges out of the hydrophobic bilayer core while simultaneously shielding the hydrophobic alkane backbone within the bilayer as schematically illustrated in Figure 1. Similar snorkeling behavior occurs in transmembrane proteins where arginine residues bend toward the lipid–water inter-face.^{22,24} The available free volume in the ligand monolayer is reduced as the AuNP core diameter increases, so we expect there will be a maximum size above which snorkeling is strongly inhibited and insertion is no longer observed. Increasing the particle diameter also increases the amount of hydrophobic surface area initially exposed to water and hence the magnitude of the driving force for insertion. The competition between these effects implies that the propensity for AuNP insertion will be maximized at an intermediate core size. Our combined experimental and simulation results show strong evidence to support this hypothesis, demonstrating for the first time that anionic AuNPs can insert into and fuse with lipid bilayers despite their highly charged surfaces and aqueous solubility.

To elucidate the interactions of striped AuNPs with cellular membranes, we synthesized lipid vesicles to serve as a model system for nonspecific AuNP-lipid interactions. Single-component giant multilamellar vesicles (GMVs) were first formed from the zwitterionic lipid DOPC. DOPC stock solutions were prepared in chloroform and gently dropped onto lightly scratched glass. The chloroform was allowed to evaporate overnight and the resulting lipid films were hydrated in water vapor at 70 °C for 6 h. Following this step, the lipid films were bathed in 50 mM sucrose and the vesicles were allowed to form overnight also at 70 °C. Vesicles were harvested gently and allowed to cool to room temperature.

AuNPs were prepared with a monolayer composed of a 1:1 mixture of 11-mercaptopundecane sulfonate (MUS) and octanethiol (OT) ligands, the same ligands previously shown to separate into stripelike domains and to encourage cellular penetration.^{7,9,12} AuNPs were prepared with the one-phase Brust synthesis according to previous methods²⁵ and labeled with a red fluorescent BODIPY dye. More details are provided in the Supporting Information. The mean core diameter of these 1:1 MUS:OT particles was 2.2 nm (see Figure S1 in Supporting Information). An external medium of 5 µg/mL calcein, a green fluorescent dye that does not passively diffuse through lipid bilayers, and 0.3 mg/mL BODIPY-labeled AuNPs in 50 mM glucose was also added to the vesicle solution. The solution was allowed to equilibrate for 1–3 h before confocal imaging.

Differential interference contrast (DIC) and confocal images of the solution are shown in Figure 2. From these images, it is apparent that green calcein fluorescence was confined to the external solution and was not observed within vesicles. In contrast, red BODIPY fluorescence from the particles was observed to colocalize with the outer bilayer of the

vesicles. Inner membranes within the multilamellar vesicles were also clearly outlined by red fluorescence as indicated by the boxed vesicles in Figure 2 and confirmed by the DIC images. Observation of individual multilamellar vesicles by transmission electron microscopy (TEM) confirmed the BODIPY signature reflected AuNPs within the bilayers (Supporting Information Figure S2). The DIC images and TEM further establish that those vesicles showing AuNP fluorescence throughout the vesicle core were GMVs composed of solid stacked layers of lipid, while unilamellar vesicles showed little/no free AuNP fluorescence in their interior, suggesting that particles preferentially embedded within available membranes. Similar results were obtained with particles of similar core diameter and all-MUS and 2:1 MUS:OT surface compositions (Supporting Information Figure S3).

These observations imply several important findings. First, the exclusion of calcein from the vesicle interior indicates that AuNPs do not disrupt the bilayer, agreeing with the nondisruptive mechanism observed in cells. Second, the localized BODIPY fluorescence from vesicle membranes, in comparison to the relatively weak background fluorescence, shows that the particles have a strong affinity for the lipid bilayer itself. Finally, the BODIPY fluorescence from inner membranes in the multilamellar vesicles confirms that the particles can access inner membranes without the aid of an endocytic mechanism.

To further probe the interactions between vesicles and AuNPs, multilamellar vesicles were prepared from a mixture of DOPC (80 mol %) and DOPS (20 mol %) lipids in 50 mM sucrose and imaged in 50 mM glucose. The inclusion of DOPS, an anionic lipid, led to a negative charge at vesicle surfaces. Figure 3 shows confocal microscopy images of BODIPY-labeled 1:1 MUS:OT particles and calcein added to DOPC–DOPS vesicles in the absence of salt (left) and in 150 mM NaCl (right). This salt concentration was chosen to mimic a typical biological environment. In both salt concentrations, calcein was still excluded from the vesicle interior. In the absence of salt, BODIPY fluorescence was only weakly observed from vesicle membranes compared to the background. This control provides further evidence that the BODIPY signal observed within GMVs above was not due to free dye in the particle suspension. In the presence of physiological levels of salt, BODIPY fluorescence was again observed from both internal and external vesicle membranes, similar to what was observed for pure DOPC. The addition of salt screened electrostatic interactions, reducing the repulsion between the anionic particles and like-charged vesicles. The occurrence of localized fluorescence, and thus some form of bilayer-particle interaction, is striking because previous simulation and experimental studies have shown that electrostatic interactions attract anionic AuNPs to the bilayer surface, even in zwitterionic membranes.^{26,27} Similarly, electrostatic-mediated surface adsorption leads to the penetration of cationic peptides.² By contrast, in this system AuNPs were observed to colocalize with bilayers even when electrostatic interactions were highly screened.

The vesicle results suggest that anionic, monolayer-protected AuNPs were capable of stably interacting with bilayers in a nondisruptive manner, while still passing through outer bilayers and interacting with inner membranes of sealed multilamellar vesicles. The observation of this same behavior in the presence of high salt concentrations and anionic lipids further suggests that membrane fusion was not mediated by electrostatic interactions, as would be expected for cationic cell-penetrating peptides or cationic AuNPs. These results

support the hypothesis of AuNP fusion driven by the hydrophobic effect. Indeed, the confocal images shown in Figures 2 and 3 are similar to images of purely hydrophobic nanoparticles reported in the literature that are known to embed within the hydrophobic bilayer core;²⁸ however, here we study soluble, anionic AuNPs that would not be expected to embed within the hydrophobic bilayer core given their highly charged surfaces, yet still demonstrate characteristics similar to purely hydrophobic AuNPs. Similar results have also been reported recently for the incorporation of block copolymer-decorated nanoparticles into block copolymer vesicles²⁹ as well as the incorporation of charged ligand-protected nanoparticles into surfactant vesicles,³⁰ providing evidence of the generality of this mechanism.

To explain the experimental observations, we developed a new model to analyze the free energy change for embedding an AuNP within a lipid bilayer with particular interest in understanding the role of hydrophobic interactions in driving insertion. The model calculates the free energy change for moving an isolated particle in solution to the bilayer midplane with no consideration for the dynamics of translocation. The total free energy change of the system, G_{tot} , results from a competition between the hydrophobic driving force and the unfavorable penalties for charge insertion, bilayer deformation, electrostatic repulsion, and the reduction of ligand entropy, which is written as:

$$\Delta G_{tot} = \Delta G_{phob} + \Delta G_{philic} + \Delta E_{elec} + \Delta E_{thick} - T\Delta S_{conf} \quad (1)$$

This free energy decomposition is similar to approaches used to study the thermodynamics of membrane protein folding.³¹ We modeled the AuNP and monolayer using a united atom representation where ligands were treated as flexible chains of hard spheres as illustrated in Figure 4A. The bilayer was modeled implicitly with the cost of charge insertion, G_{philic} , estimated from previous atomistic simulations that calculated the free energy barrier for transferring negative charges into the nonpolar bilayer core.³² This penalty includes the cost for the formation of a water defect in the bilayer and interactions with lipid head groups as these effects were captured in the source study from which the potential was drawn. The magnitude of the hydrophobic effect, G_{phob} , was estimated by explicitly calculating the solvent-accessible surface area (SASA) of hydrophobic beads in the system. The magnitude of the hydrophobic effect has been shown to scale approximately linearly with the SASA in studies of alkane transfer into aqueous solvent;²⁰ here we calculated the reduction in the SASA upon insertion and scaled by a phenomenological parameter of 47 cal/mol/Å² to approximate G_{phob} .³³ Electrostatic interactions between charged end groups, E_{elec} , were captured using a screened Coulomb potential consistent with Debye–Huckel theory.³⁴ The conformational entropy change of the ligands, S_{conf} , was calculated using the Bennett Acceptance Ratio (BAR) approach, allowing the change in free energy of the system to be calculated as the thickness of the bilayer was systematically increased from zero (baseline) to a final value.³⁵ For each thickness, the complete free energy change relative to the baseline was calculated using Monte Carlo simulations, and an additional analytical term related to the cost for bilayer deformation, E_{thick} , was included.³⁶ In all simulations, the temperature was set to 300 K and the salt concentration to 150 mM to match experimental conditions. Figure 4A shows example simulation snapshots of the particle in the aqueous

and embedded state, with the SASA explicitly drawn as a blue surface. The computational efficiency of this model allowed for the comparison between AuNPs of different sizes, monolayer compositions, and monolayer morphologies. Further details on the simulation methodology along with additional simulation snapshots are included in the Supporting Information (Figures S4–S6).

To match previous cell experiments^{7,12} and the vesicle experiments discussed above, the free energy changes for the insertion of particles with monolayer compositions of all-MUS, 2:1 MUS:OT, and 1:1 MUS:OT in random, striped, and perfectly mixed morphologies were calculated. Figure 4B shows images of the morphologies simulated. For each combination of surface composition and morphology, the particle gold core diameter was varied between 1.0 and 10.0 nm with resulting free energy changes shown in Figure 4C. As predicted, the free energy change for each particle type was a nonmonotonic function of diameter with preferred core diameters at intermediate sizes where insertion was strongly favored followed by a sharp increase in the free energy until the overall change was positive, indicating a maximum cutoff diameter for stable insertion. The width and depth of the free energy curves shifted dramatically when the surface composition was altered; all-MUS particles only had negative free energy changes for diameters less than 3.5 nm, while adding more hydrophobic ligands to the surface increased both this embedding cutoff and the magnitude of the free energy change. However, there was no apparent difference in the free energy change for embedding between the three different morphologies as would be expected from cellular penetration experiments. All three morphologies, stripes, random, and mixed, showed nearly identical results, reflecting a minimal change in the free energy when ligand positions were switched on the AuNP surface.

These fusion results can be understood by considering the relative magnitude of the hydrophobic driving force and the ability of the protecting monolayer to deform to minimize the unfavorable insertion of charges into the bilayer core. The simulations show that insertion critically depends on ligands deforming to snorkel charged end groups to the nearest aqueous interface while simultaneously increasing the amount of hydrophobic surface area exposed to the bilayer core as shown in Figure 4A. This ligand snorkeling, especially in the case of all-MUS particles, is what allows the charged surfaces to appear largely hydrophobic to the bilayer core, indicating that ligand flexibility is a critical factor that determines if fusion is favorable. Because the ligand domains were small, the relative positioning of hydrophilic and hydrophobic ligands on the surface did not significantly affect the ability of the ligands to snorkel and hence there was no observed morphology distinction. Much more important than the surface morphology were the diameter of the AuNP and the composition of ligands in the monolayer. For smaller particle diameters, the monolayer contained a large amount of free volume, maximizing ligand fluctuations and minimizing the barrier to snorkeling. When the AuNP diameter was large, however, the volume accessible to each ligand decreased as the radius of curvature of the NP surface increased, inhibiting ligand deformation. The ligands were thus forced into more undesirable configurations where charged end groups were exposed to the bilayer core leading to an overall increase in the system free energy that dominated the favorable hydrophobic term. Increasing the relative proportion of hydrophilic ligands also inhibited insertion by imposing a barrier to ligand bending due to the bulkiness of the sulfonate end groups and increased

electrostatic repulsion. Finally, AuNP monolayers with additional hydrophobic ligands had larger amounts of exposed hydrophobic surface area in the baseline state that was shielded in the bilayer, leading to a greater hydrophobic driving force. The combination of these factors led 1:1 MUS:OT particles to prefer embedding more strongly than 2:1 MUS:OT and all-MUS particles, independent of surface morphology. These simulations suggest that monolayer composition and particle size, not actual morphology, control the thermodynamics of fusion with lipid bilayers. We must stress, however, that these results reflect only the free energy change between an isolated AuNP in solvent and an AuNP inserted into the bilayer, and do not take into account any role of morphology in governing the kinetics of translocation. Describing the kinetics of bilayer penetration is beyond the scope of this work, but morphology may play a critical role in determining the likelihood of insertion.

The simulations yielded free energy curves that predict a strong size and surface composition dependence for particle insertion. To compare to simulation results, size-fractionated samples of AuNPs²⁵ with different monolayer compositions were added to a DOPC “black” lipid membrane (BLM). The BLM was assembled over a pore dividing two water reservoirs with 50 mM KCl in an electrochemical cell. The quantity of embedded AuNPs was measured by calculating the change in the capacitance of the black lipid membrane upon the addition of particles to one of the two solvent reservoirs as described recently.³⁷ For particle samples that interacted with the bilayer, increasing the concentration of particles in the solution increased the capacitance of the bilayer until it eventually reached a plateau. Adding additional particles to the other solvent reservoir failed to increase the capacitance change once the plateau was reached. This observation supports the insertion mechanism, as the capacitance should continue to increase as particles were added to both sides of the bilayer if surface adsorption led to a capacitance change. This technique also allowed particle fusion to be measured for nonfluorescently labeled particles; however, the results were unchanged when BODIPY was conjugated to the AuNP surfaces. Additional details on this methodology can be found in ref 37.

Using this method, all-MUS, 1:1 MUS:OT and 1:1 MUS:OT particles of different size fractions were prepared and added independently to the BLM apparatus. For each particle composition, a threshold particle size fraction was determined where no capacitance change was observed at all. As predicted by simulations, the 2:1 MUS:OT particles had a smaller cutoff threshold than 1:1 MUS:OT. No fraction of all-MUS was observed to induce a capacitance change, but fractions with sizes smaller than the predicted cutoff could not be reliably synthesized in sufficient quantity for the BLM experiments.³⁷ A comparison between the size thresholds obtained from experiments and those predicted by the simulations is shown in Figure 4D with experimental core sizes estimated from the hydrodynamic radii measured for each particle fraction with 3.1 nm subtracted to approximate the size of the monolayer.⁷ The simulation and experimental results show remarkable agreement, reinforcing support for the insertion hypothesis.

To test whether the penetration of AuNPs into cells is also size-dependent, we size-fractionated consecutively sized all-MUS AuNP batches, a surface composition previously shown not to penetrate into cells via the energy-independent mechanism.^{7,12} Five fractions

with average gold core diameters ranging from 2.4 to 5.8 nm (see Figure 5) and a concentration of 0.3 mg/mL were fluorescently labeled with a BODIPY dye as in previous experiments. To test for the existence of free dye, the NP fractions were first incubated with red blood cells (RBCs), employing a recent protocol we developed for the presence of free dye.³⁸ Any fractions found to have free dye were not used. Each of the 5 fractions was then incubated with HeLa cells cultured following previously used methods^{12,38} at both 37 and 4 °C for 3 h. The median fluorescence intensity (MFI) of BODIPY fluorescence for each fraction was analyzed using flow cytometry with corresponding two-dimensional dot plots shown in Supporting Information Figure S7. Complementary measurement using confocal imaging of particle uptake was performed with live cells using a Zeiss LSM 700 Inverted Microscope to visually confirm that dye was localized to the cell cytosol, indicating that increased BODIPY fluorescence was due to AuNP internalization. Representative confocal images taken after three washes in media and at the 3 h time point are shown in Figure S8 of the Supporting Information.

Figure 5 shows the BODIPY MFI averaged over three biological replicates as a function of particle size. For both temperatures, the average MFI was observed to decrease with larger particle sizes indicating a decrease in AuNP internalization. The average MFI reached a plateau value for batch C consisting of particles of mean diameter 3.4 nm, near the size threshold identified in Figure 4. The observation of intracellular fluorescence in excess of the control even at 4 °C, where endocytosis is inhibited, indicates that penetration occurred by an energy-independent mechanism consistent with previous observations for 2:1 MUS:OT and 1:1 MUS:OT particles.^{7,12} The decrease in fluorescence intensity with larger particle batches correlates with the size-dependence shown for pure bilayer systems (c.f. Figure 4) and indicates that the previous observation of no penetration by all-MUS particles may be due to the larger sizes studied in previous work (≈ 4.5 nm core diameter⁷). These findings provide support for the hypothesis that membrane insertion is a critical step in the cell penetration pathway.

The agreement between simulations and both vesicle and black lipid membrane experiments shows that AuNPs are capable of inserting into bilayers depending on particle size and monolayer composition. Insertion is possible due to the deformation of the ligand shell, relying on the flexibility at the interface granted by significant curvature of the AuNP core. The combined experimental and simulation results showed that AuNPs with small core diameters preferentially fused with the bilayer with a varying size threshold depending on the composition of the monolayer. Experiments with negatively charged bilayers also showed that fusion occurred even when electrostatic interactions were highly screened, though electrostatics may affect the kinetics of AuNP insertion.

Our results indicate that there is a correlation between the AuNPs best suited for embedding in model lipid bilayers and the AuNPs that nondisruptively penetrate cells. In previous cell experiments, striped 2:1 MUS:OT particles penetrated in the greatest quantities while all-MUS particles showed minimal signs of penetration.⁷ These results match the size thresholds identified here; the 2:1 MUS:OT particles had a significantly larger cutoff size than all-MUS particles, while the vesicle studies determined that both particle types were able to access the interior of multilamellar vesicles. Given that the particle samples used in

the cell experiments were polydisperse with mean diameters of about 4.5 nm,⁷ the differences in cellular uptake may correlate with the number of particles in each sample with diameters less than the cutoff diameter, supporting the hypothesis that bilayer fusion is the critical intermediate step in membrane penetration. Our results further suggest that bilayer fusion is favorable for sufficiently small AuNP core diameters independent of surface composition for the amphiphilic ligands considered here. We confirmed this finding by demonstrating the preferential uptake of small all-MUS particle batches at both 37 and 4 °C, in contrast to the observation of no penetration in previous studies of larger all-MUS samples. Finally, the general preference of small AuNPs for cellular penetration is supported by recent experimental results reported in the literature showing the nonendocytotic uptake of small AuNPs (gold core diameter 1.6 nm) with a variety of surface coatings.³⁹

The magnitude of the free energy changes calculated from simulations can be put in context by comparing to related systems. A recent coarse-grained molecular dynamics simulation of charged alkanethiol-protected AuNPs determined that 2.2 nm particles exhibit a free energy minimum of approximately -30 kcal/mol at the surface of DOPC bilayers.²⁶ This free energy minimum was calculated in the absence of salt and was primarily attributed to electrostatic interactions; the magnitude of the minimum would decrease at physiological salt concentrations. In this work, the free energy change for an all-MUS particle with a diameter of 2.0 nm was -40.3 kcal/mol, resulting in a more stable free energy minimum for particle insertion than for surface adsorption. For larger, mixed monolayer particles, we predicted free energy changes as large as -171 kcal/mol for 3.5 nm 2:1 MUS:OT particles and -288 kcal/mol for 4.5 nm 1:1 MUS:OT particles. These values are comparable in magnitude to the unfolding free energy of multimeric transmembrane proteins calculated from the reversible extraction of folded proteins from membranes in single-molecule pulling experiments.^{40,41} This unfolding free energy has been measured as 162.3 kcal/mol for halorhodopsin (HR) and 290.5 kcal/mol for bacteriorhodopsin (BR),⁴² values similar to the maximum free energy changes measured here. These values correspond to free energy changes of 0.92 kcal/mol per amino acid for HR and 1.32 kcal/mol per amino acid for BR, values again comparable to 0.93 kcal/mol per ligand for 2:1 MUS:OT and 0.95 kcal/mol per ligand for 1:1 MUS:OT. These values also compare well to the free energy for insertion of individual amino acids as measured by biological hydrophobicity scales.^{6,21} The simulations thus predict that the total insertion free energy is on par with that measured by highly stable membrane proteins and well in excess of the expected free energy change for surface adsorption. However, unlike membrane proteins, the AuNPs insert spontaneously from aqueous solution rather than being inserted by the translocon apparatus,²¹ a result that could be used to guide the design of synthetic AuNPs to mimic transmembrane proteins.

Given that the magnitude of the calculated free energy change is lower than what is known for transmembrane proteins, it is possible that AuNPs can repeatedly insert into and withdraw from the bilayer over experimental time scales. However, we did not consider the kinetics of embedding here, and as a result the full mechanism of penetration is still subject to additional study. The mechanism of penetration may involve a transient increase in membrane permeability,⁴³ lipid rearrangement similar to a vesicle fusion event,⁴⁴ or the existence of spontaneous membrane defects, which are prominent in biological membranes.^{45,46} Translocation may also occur by a multiple state pathway similar to what is

proposed for the insertion of membrane proteins or antimicrobial peptides, where particles first bind to the surface before inserting into the preferred transmembrane state.^{1–3,31} It is unclear what role surface morphology, which was shown here to not affect the embedded state, may play in membrane insertion dynamics. It is also unclear whether the particle surface may be modified by place exchange reactions upon cellular internalization and if this plays a critical role in biasing penetration into cells.⁴⁷ In future work, we will explore these questions, determine the influence of embedded AuNPs on the phase behavior of surrounding lipids, and establish a methodology for designing particle surfaces optimized for bilayer fusion. This work represents a critical first step in fully understanding the interactions between monolayer-protected AuNPs and cells by demonstrating the nondisruptive nature of the inserted state and showing the importance of AuNP surface properties. In particular, we show that fusion is most favorable when ligands are able to easily fluctuate to adjust to the bilayer, allowing charges to snorkel out of the membrane and effectively rearranging the surface of the AuNP to appear locally hydrophobic to the bilayer environment.¹³ Understanding the role of such surface properties in insertion may also help explain nonspecific penetration observed in similar systems such as quantum dots.⁴⁸ The amphiphilic monolayers of the AuNPs described here are also strikingly similar to the pattern of hydrophobic and charged residues found in cell-penetrating peptides⁴⁹ which may provide some insight into the mechanism of penetration of these biological molecules as well.

Supplementary Material

Refer to Web version on PubMed Central for supplementary material.

Acknowledgments

R.C.V. is supported in part by a National Science Foundation Graduate Research Fellowship. R.C.V. and A.A.K. also acknowledge support by the MRSEC Program of the National Science Foundation under award number DMR-0819762. P.U.A. and D.J.I. acknowledge support under award number U54CA143874 from the National Cancer Institute and the U.S. Army Research Office under contracts W911NF-13-D-0001 and W911NF-07-D-0004. T.O. 8. D.J.I. is an investigator of the Howard Hughes Medical Institute. R.P.C. and F.S. acknowledge support from the Swiss National Foundation NRP 64 Program. Some of the computations in this paper were run on the Odyssey cluster supported by the FAS Sciences Division Research Computing Group. This work used the Extreme Science and Engineering Discovery Environment (XSEDE), which is supported by National Science Foundation grant number OCI-1053575. The authors also thank T. Carney for assistance with flow cytometry measurements.

REFERENCES

1. Shai Y. *Biochim. Biophys. Acta, Biomembr.* 1999; 1462:55–70.
2. Hecce HD, Garcia AE. *Proc. Natl. Acad. Sci. U.S.A.* 2007; 104:20805–20810. [PubMed: 18093956]
3. Yesylevskyy S, Marrink S-J, Mark AE. *Biophys. J.* 2009; 97:40–49. [PubMed: 19580742]
4. Chen J, Hessler JA, Putschakayala K, Panama BK, Khan DP, Hong S, Mullen DG, DiMaggio SC, Som A, Tew GN, Lopatin AN, Baker JR, Holl MMB, Orr BG. *J. Phys. Chem. B.* 2009; 113:11179–11185. [PubMed: 19606833]
5. Leroueil PR, Berry SA, Duthie K, Han G, Rotello VM, McNerny DQ, Bakera, Orr BG, Banaszak Holl MM. *Nano Lett.* 2008; 8:420–424. [PubMed: 18217783]
6. White SH, Wimley WC. *Annu. Rev. Biophys. Biomol. Struct.* 1999; 28:319–365. [PubMed: 10410805]

7. Verma A, Uzun O, Hu Y, Han H-S, Watson N, Chen S, Irvine DJ, Stellacci F. *Nat. Mater.* 2008; 7:588–595. [PubMed: 18500347]
8. Jewell CM, Jung J-M, Atukorale PU, Carney RP, Stellacci F, Irvine D. *J. Angew. Chem., Int. Ed.* 2011; 50:12312–12315.
9. Jackson AM, Myerson JW, Stellacci F. *Nat. Mater.* 2004; 3:330–336. [PubMed: 15098025]
10. Jackson AM, Hu Y, Silva PJ, Stellacci F. *J. Am. Chem. Soc.* 2006; 128:11135–11149. [PubMed: 16925432]
11. Carney RP, DeVries GA, Dubois C, Kim H, Kim JY, Singh C, Ghorai PK, Tracy JB, Stiles RL, Murray RW, Glotzer SC, Stellacci F. *J. Am. Chem. Soc.* 2007; 130:798–799. [PubMed: 18154337]
12. Carney RP, Carney TM, Mueller M, Stellacci F. *Biointerphases.* 2012; 7:17. [PubMed: 22589060]
13. Van Lehn RC, Alexander-Katz A. *Soft Matter.* 2011; 7:11392.
14. Li Y, Li X, Li Z, Gao H. *Nanoscale.* 2012; 4:3768–3775. [PubMed: 22609866]
15. Prates Ramalho JP, Gkeka P, Sarkisov L. *Langmuir.* 2011; 27:3723–3730. [PubMed: 21391652]
16. Makarucha AJ, Todorova N, Yarovsky I. *Eur. Biophys. J.* 2011; 40:103–115. [PubMed: 21153635]
17. Nel AE, Madler L, Velegol D, Xia T, Hoek EMV, Somasundaran P, Klaessig F, Castranova V, Thompson M. *Nat. Mater.* 2009; 8:543–557. [PubMed: 19525947]
18. Moyano DF, Rotello VM. *Langmuir.* 2011; 27:10376–10385. [PubMed: 21476507]
19. Verma A, Stellacci F. *Small.* 2009; 6:12–21. [PubMed: 19844908]
20. Chandler D. *Nature.* 2005; 437:640–647. [PubMed: 16193038]
21. Hessa T, Kim H, Bihlmaier K, Lundin C, Boekel J, Andersson H, Nilsson I, White SH, Heijne G. *Nature.* 2005; 433:377–381. [PubMed: 15674282]
22. Dorairaj S, Allen TW. *Proc. Natl. Acad. Sci. U.S.A.* 2007; 104:4943–4948. [PubMed: 17360368]
23. Lane JMD, Grest GS. *Phys. Rev. Lett.* 2010; 104:235501. [PubMed: 20867251]
24. Strandberg E, Killian JA. *FEBS Lett.* 2003; 544:69–73. [PubMed: 12782292]
25. Carney RP, Kim JY, Qian H, Jin R, Mehenni H, Stellacci F, Bakr OM. *Nat. Commun.* 2011; 2:335. [PubMed: 21654635]
26. Lin J, Zhang H, Chen Z, Zheng Y. *ACS Nano.* 2010; 4:5421–5429. [PubMed: 20799717]
27. Wang B, Zhang L, Bae SC, Granick S. *Proc. Natl. Acad. Sci. U.S.A.* 2008; 105:18171–18175. [PubMed: 19011086]
28. Von White G, Chen Y, Roder-Hanna J, Bothun GD, Kitchens CL. *ACS Nano.* 2012; 6:4678–4685. [PubMed: 22632177]
29. Mai Y, Eisenberg A. *J. Am. Chem. Soc.* 2010; 132:10078–10084. [PubMed: 20608678]
30. Lee H-Y, Shin SHR, Abezgauz LL, Lewis SA, Chirsan AM, Danino DD, Bishop KJM. *J. Am. Chem. Soc.* 2013; 135:5950–5953. [PubMed: 23565704]
31. Ben-Tal N, Ben-Shaul A, Nicholls A, Honig B. *Biophys. J.* 1996; 70:1803–1812. [PubMed: 8785340]
32. MacCallum JL, Bennett WFD, Tieleman DP. *J. Gen. Physiol.* 2007; 129:371–377. [PubMed: 17438118]
33. Sharp KA, Nicholls A, Fine RF, Honig B. *Science.* 1991; 252:106–109. [PubMed: 2011744]
34. Guo P, Sknepnek R, Olvera de la Cruz M. *J. Phys. Chem. C.* 2011; 115:6484–6490.
35. Bennett CH. *J. Comput. Phys.* 1976; 22:245–268.
36. Nielsen C, Goulian M, Andersen OS. *Biophys. J.* 1998; 74:1966–1983. [PubMed: 9545056]
37. Carney RP, Astier Y, Carney TM, Voitchovsky K, Jacob Silva PH, Stellacci F. *ACS Nano.* 2013; 7:932–942. [PubMed: 23267695]
38. Andreozzi P, Martinelli C, Carney RP, Carney TM, Stellacci F. *Mol. Pharmacol.* 2013; 10:875–882.
39. Lund T, Callaghan MF, Williams P, Turmaine M, Bachmann C, Rademacher T, Roitt IM, Bayford R. *Biomaterials.* 2011; 32:9776–9784. [PubMed: 21944722]
40. Oesterhelt F, Oesterhelt D, Pfeiffer M, Engel A, Gaub HE, Mueller DJ. *Science.* 2000; 288:143–146. [PubMed: 10753119]

41. Kessler M, Gottschalk KE, Janovjak H, Muller DJ, Gaub HE. *J. Mol. Biol.* 2006; 357:644–654. [PubMed: 16434052]
42. Preiner J, Janovjak H, Rankl C, Knaus H, Cisneros DA, Kedrov A, Kienberger F, Muller DJ, Hinterdorfer P. *Biophys. J.* 2007; 93:930–937. [PubMed: 17483176]
43. Pogodin S, Werner M, Sommer J-U, Baulin VA. *ACS Nano.* 2012; 6:10555–10561. [PubMed: 23128273]
44. Chernomordik LV, Kozlov MM. *Nat. Struct. Mol. Biol.* 2008; 15:675–683. [PubMed: 18596814]
45. Leontiadou H, Mark AE, Marrink SJ. *Biophys. J.* 2004; 86:2156–2164. [PubMed: 15041656]
46. Ting CL, Wang Z-G. *Soft Matter.* 2012; 8:12066–12071.
47. Zhu Z-J, Tang R, Yeh Y-C, Miranda OR, Rotello VM, Vachet RW. *Anal. Chem.* 2012; 84:4321–4326. [PubMed: 22519403]
48. Wang T, Bai J, Jiang X, Nienhaus GU. *ACS Nano.* 2012; 6:1251–1259. [PubMed: 22250809]
49. Marks JR, Placone J, Hristova K, Wimley WC. *J. Am. Chem. Soc.* 2011; 133:8995–9004. [PubMed: 21545169]

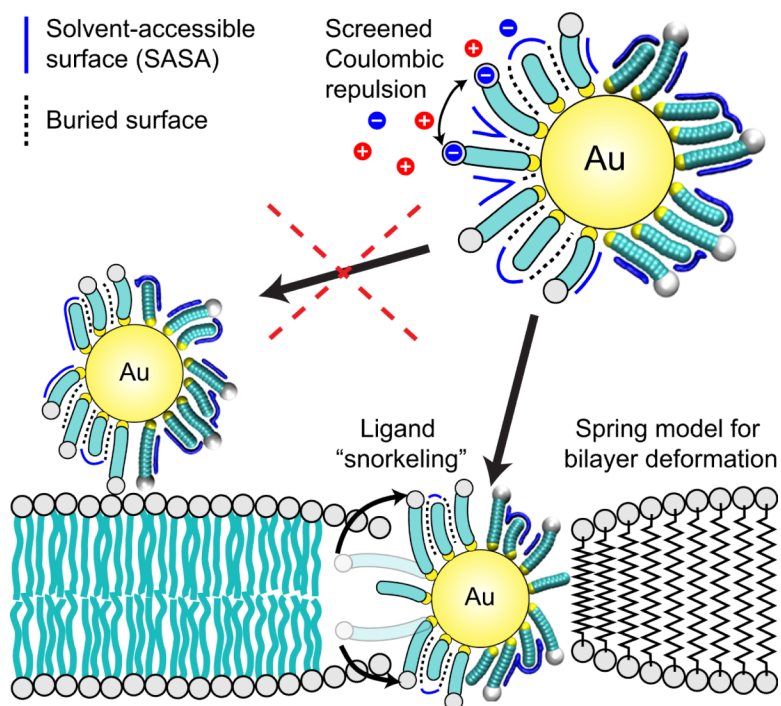


Figure 1. Schematic illustration accompanied by partial simulation snapshots of the proposed interaction between AuNPs and the bilayer. Rather than adopt a surface-adsorbed state due to electrostatic interactions, the particles insert into and fuse with the bilayer. The driving force for fusion is the reduction of hydrophobic alkane surface area exposed to water (drawn as blue lines in both the schematic and simulation snapshots) upon transferring the particle into the hydrophobic bilayer core. To stabilize the transmembrane state, the ligands deform to snorkel charges out of the bilayer. The springlike bilayer also deforms to match the hydrophobic surface of the embedded AuNP.

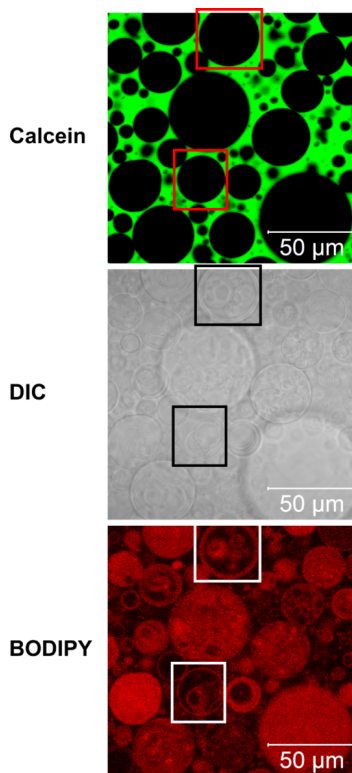


Figure 2. Confocal microscopy images of BODIPY-labeled 1:1 MUS:OT AuNPs in solution with multilamellar single-component DOPC vesicles and the membrane impermeable dye calcein. Green fluorescence from calcein was only observed from the vesicle exterior, while red BODIPY fluorescence was localized to both interior and exterior membranes of the multilamellar vesicles. BODIPY fluorescence from membranes was noticeably stronger than the background, indicating a preferential bilayer-AuNP interaction. Boxes are drawn around vesicles with distinct inner membranes by comparison of the calcein, DIC, and BODIPY images.

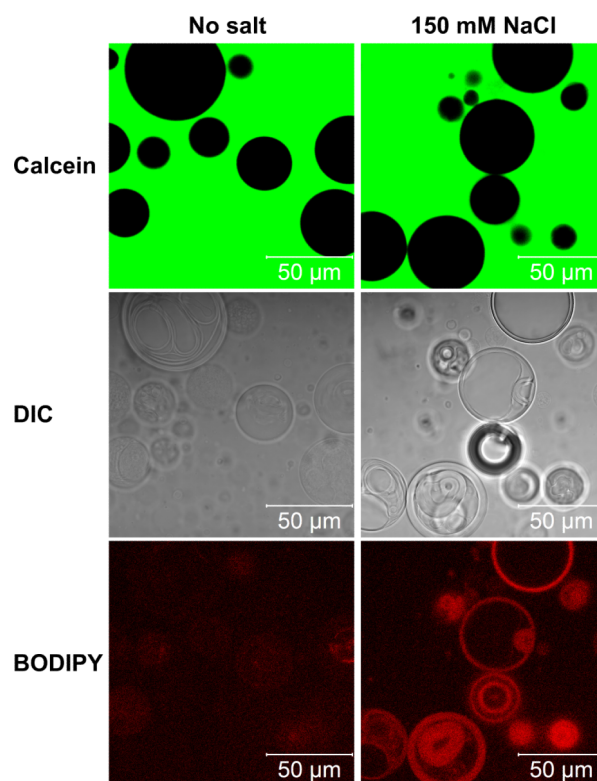
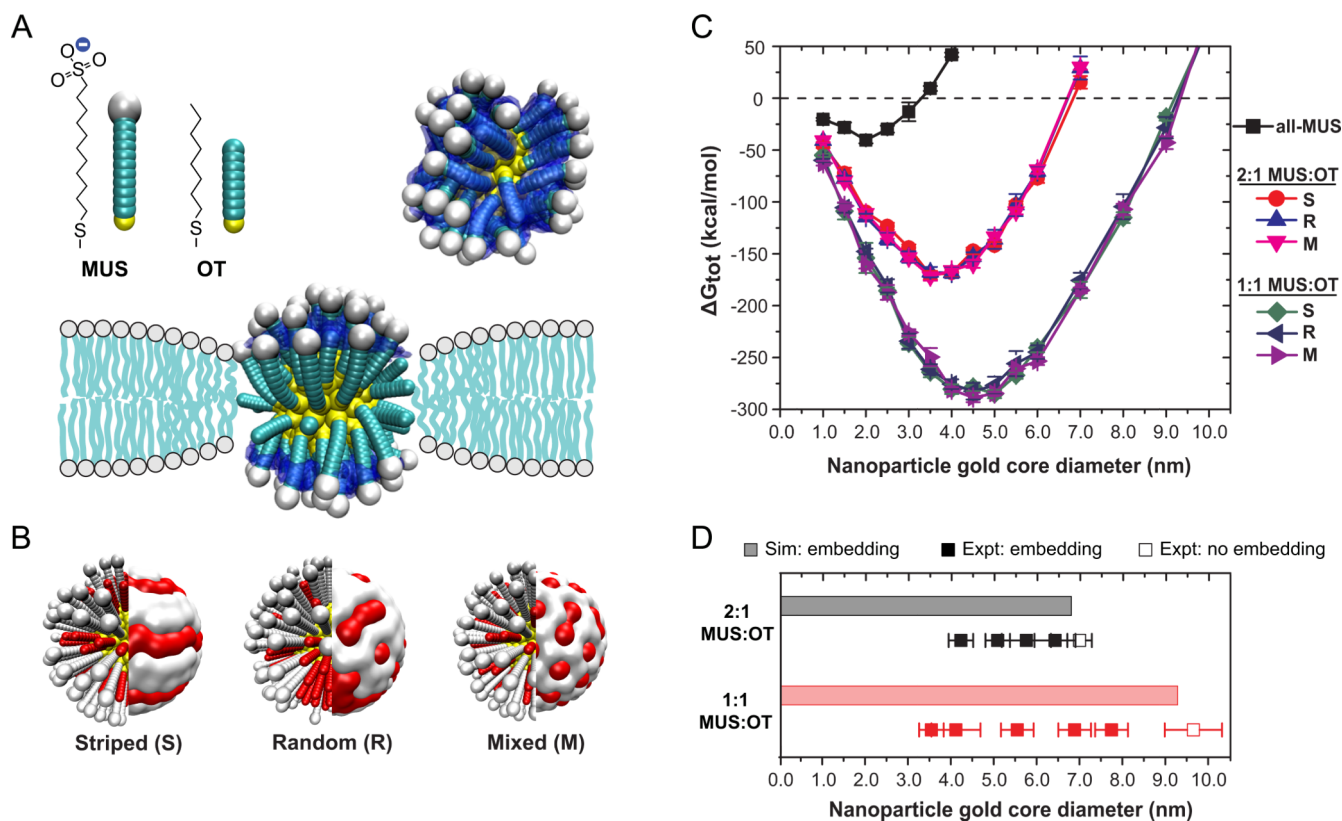


Figure 3.

Confocal images of BODIPY-labeled 1:1 MUS:OT AuNPs in solution with multilamellar, anionic DOPC/DOPS vesicles without salt (left) and 150 mM NaCl (right). In the absence of salt, the BODIPY fluorescence from vesicles was barely discernible from background fluorescence, consistent with like-charge repulsion between the anionic AuNPs and anionic vesicles. Upon adding salt, fluorescence was again clearly observed from both external and interior membranes in the multilamellar vesicles, consistent with observations of pure DOPC vesicles.

**Figure 4.**

Simulation results and comparison to experiments. (A) United atom simulation model based on explicit calculation of solvent-accessible surface area (SASA). The bilayer was considered implicitly and biases the conformations of ligands by reducing the SASA and penalizing the insertion of charges into the membrane interior. The SASA is drawn as a blue surface. (B) Illustration of the three surface morphologies simulated. (C) Simulation results graphed as the change in free energy for embedding as a function of AuNP core diameter. The free energy change was a strong function of particle diameter and monolayer composition, but not surface morphology. The dashed line indicates where the total free energy change is 0, indicating the maximum diameter where embedding would be preferred. (D) Comparison of simulation results from (C) to black lipid membrane experiments. Size-fractionated AuNP samples interacted with black lipid membranes depending on particle size. Filled-in squares indicate experimental particle fractions that induced a capacitance change in the membranes, while empty squares indicate particle fractions that did not. Error bars show the deviation in particle size.

Nanoparticle batch	Mean diameter (nm)
A	2.4 ± 0.3
B	2.9 ± 0.5
C	3.4 ± 0.8
D	4.9 ± 1.1
E	5.8 ± 1.4

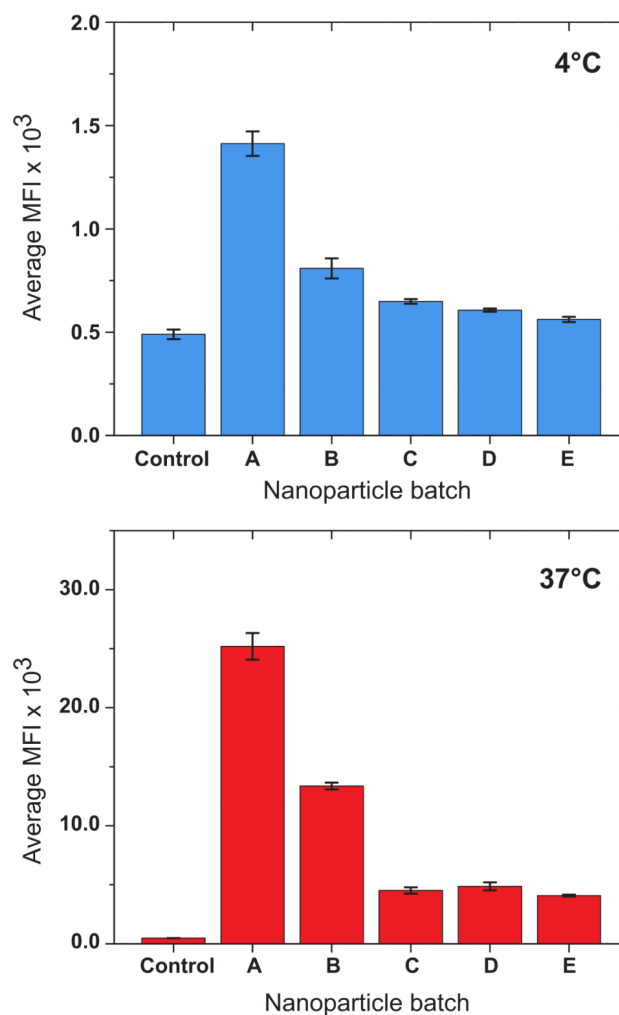


Figure 5.

Flow cytometry was used to measure cellular uptake of all- MUS particles as a function of particle diameter at both 4 and 37 °C. Cellular uptake was measured by the median fluorescence intensity of BODIPY-labeled AuNPs confined to the cytosol. Five batches of all- MUS particles of increasing average particle diameter were synthesized and added to HeLa cells. At both temperatures, the batches with average sizes below the size threshold identified in Figure 4 (batches A and B) penetrated in greater quantities than the larger particle batches. At 4 °C, where endocytosis is inhibited, the observation of penetration indicates that all-MUS particles enter via a nonendocytotic mechanism